Does Infall End Before the Class I Stage?

Erik M. Gregersen[1]
Department of Physics and Astronomy, McMaster University, Hamilton, ON L8S 4M1, Canada and
Department of Astronomy, California Institute of Technology, MS 105-24, Pasadena, CA 91125

Neal J. Evans II[2]
Department of Astronomy, The University of Texas at Austin, Austin, TX 78712–1083

Diego Mardones[3]
Departamento de Astronomia, Universidad de Chile, Casilla 36-D, Santiago, Chile

Philip C. Myers[4]
Harvard-Smithsonian Center for Astrophysics, 60 Garden Street, Cambridge, MA 02138

LaTeXed at 735 min., February 1, 2008

ABSTRACT

We have observed HCO^+ $J = 3-2$ toward 16 Class I sources and 18 Class 0 sources, many of which were selected from Mardones et al. (1997). Eight sources have profiles significantly skewed to the blue relative to optically thin lines. We suggest six sources as new infall candidates. We find an equal "blue excess" among Class 0 and Class I sources after combining this sample with that of Gregersen et al. (1997). We used a Monte Carlo code to simulate the temporal evolution of line profiles of optically thick lines of HCO^+, CS and H_2CO in a collapsing cloud and found that HCO^+ had the strongest asymmetry at late times. If a blue-peaked line profile implies infall, then the dividing line between the two classes does not trace the end of the infall stage.

Subject headings: stars: formation – stars: pre-main sequence - submillimeter

1. INTRODUCTION

For many years, infalling protostars were sought, but most claims of collapse were challenged. Through the discovery of a population of cold ($T_D \sim 30$ K), heavily enshrouded ($A_V \sim 1000$) objects by IRAS and groundbased telescopes, a number of protostellar candidate objects became available for study. Subsequent observations of these Class 0 sources (André et al. 1993) revealed spectral-line profiles indicative of infall in 13 objects (Walker et al. 1986; Zhou et al. 1993; Zhou et al. 1994; Moriarty-Schieven et al. 1995; Hurt et al. 1996; Myers et al. 1996; Ward-Thompson et al. 1996; Gregersen et al. 1997; Lehtinen 1997; Mardones et al. 1997). If these infall candidates actually represent infall, we can begin to study the evolution of infall by comparing line profiles of sources believed to be in different evolutionary states.

[1]Electronic mail: gregerse@physun.physics.mcmaster.ca

[2]Electronic mail: nje@astro.as.utexas.edu

[3]Electronic mail: mardones@das.uchile.cl

[4]Electronic mail: pmyers@cfa.harvard.edu

Mardones et al. observed 23 Class 0 sources ($T_{bol} < 70$ K) and 24 Class I sources ($70 \leq T_{bol} \leq 200$ K) in the optically thick H_2CO $2_{12} - 1_{11}$ and CS $J = 2 - 1$ lines and the optically thin N_2H^+ $JF_1F_2 = 101 - 012$ line. T_{bol}, the temperature of a blackbody with the same mean frequency as the observed spectral energy distribution, increases with age from the highly embedded Class 0 sources to the pre-main sequence Class III sources ($T_{bol} > 2800$ K) (Myers and Ladd 1993). The upper boundary of the Class I category is 650 K but Mardones et al. chose the most deeply embedded Class I sources to study the earliest stages of accretion. Since protostellar collapse is expected to produce double-peaked profiles in optically thick lines with the blue peak stronger than the red peak or lines that are blue-skewed relative to the velocity of an optically thin line, Mardones et al. compared the percentage of sources in each Class that displayed such asymmetry and found that the "blue excess" (the number of sources with significant blue asymmetry minus the number of sources with significant red asymmetry divided by the total number of sources) was very different for Class 0 and Class I sources: for H_2CO, 0.39 for Class 0 sources and 0.04 for Class I sources; and for CS, 0.53 for Class 0 sources and 0.00 for Class I sources. Park et al. (1999) have done a survey of Class 0 and I sources in HCN $J = 1 - 0$ and observed similar results. Using the significance criterion of Mardones et al., the blue excess is 0.27 for Class 0 sources and 0.00 for Class I sources.

We decided to observe the Class I sources studied in Mardones et al. in HCO^+ $J = 3 - 2$ for two reasons. First, the data obtained would be more easily compared with the HCO^+ Class 0 survey of Gregersen et al. (1997). Second, the HCO^+ $J = 3 - 2$ line is usually stronger and more opaque than the other lines; consequently, it may be more sensitive to infall at later stages when much of the cloud material has accreted but infall is not complete.

The sources we observed are listed in Table 1. Our sample includes 4 Class 0 sources Mardones et al. observed that were not observed by Gregersen et al. as well as 10 sources not observed by Mardones et al. but which have been identified by others as either Class 0 or early Class I.

2. OBSERVATIONS AND RESULTS

We observed 16 Class I and 18 Class 0 sources in the HCO^+ $J = 3 - 2$ line with the 10.4-m telescope of the Caltech Submillimeter Observatory (CSO)[5] at Mauna Kea, Hawaii in December 1995, September 1996, April 1997, June 1997, December 1997 and July 1998. The sources are listed in Table 1 with their celestial coordinates, distances, T_{bol} and the off position used for position switching. We used an SIS receiver (Kooi 1992). The backend was an acousto-optic spectrometer with 1024 channels and a bandwidth of 49.5 MHz. The frequency resolution was about 2 channels, which is 0.11 km s^{-1} at 267 GHz, except for the December 1995 observations when the resolution was near 3 channels or 0.16 km s^{-1} at 267 GHz. Chopper-wheel calibration was used to obtain the antenna temperature, T_A^*. The lines we observed are listed in Table 2 with their frequencies, the velocity resolution, the beamsize and the main beam efficiency, η_{mb}. The main beam efficiencies were calculated using planets as calibration sources. Data from separate runs were resampled to the resolution of the run with the worst frequency resolution before averaging. A first order baseline was removed before spectra were averaged.

Line properties are listed in Table 3. T_A^* is the peak temperature in the line profile. For single-peaked lines, V_{LSR}, the line centroid, and ΔV, the line width, were found by fitting a single Gaussian to the line

[5]The CSO is operated by the California Institute of Technology under funding from the National Science Foundation, contract AST 90–15755.

profile. For lines that have two blended peaks, we list two values of T_A^* and V_{LSR}, one for each peak, and one value for the line width, which is the width across the spectrum at the temperature where the weaker peak falls to half power.

We observed 34 sources in the HCO^+ $J = 3 - 2$ line. Nine of these sources showed blue asymmetry (Figure 1) and six showed red asymmetry (Figure 2) as determined by visual inspection of the line profiles. Nineteen sources showed no significant asymmetry (Figures 3 and 4). We observed eight sources in the $H^{13}CO^+$ $J = 3 - 2$ line, five of which showed blue asymmetry in the HCO^+ $J = 3 - 2$ line.

3. Individual Sources

IRAS03235+3004 Ladd et al. (1993) observed this source at H and K. Mardones et al. (1997) observed a red-skewed line profile in both CS and H_2CO. The HCO^+ $J = 3 - 2$ line is double-peaked with the blue peak stronger (Figure 1). Both the H_2CO and CS lines of Mardones et al. peak at the HCO^+ red peak while the N_2H^+ line peaks slightly to the blue of the HCO^+ dip. However, there is significant H_2CO and CS emission at the velocity of the blue peak.

L1455 Frerking and Langer (1982) first detected a CO outflow in this source. Submillimeter observations revealed a small dense core surrounding the exciting source (Davidson and Jaffe 1984). Goldsmith et al. (1984) observed two well-collimated outflows. Mardones et al. observed a symmetric H_2CO line. We observe a slightly blue-skewed line in HCO^+ $J = 3 - 2$ which peaks 0.5 km s^{-1} to the blue of the H_2CO line (Figure 3).

IRAS03256+3055 This source is located near the NGC1333 complex. Mardones et al. observed a red-peaked line profile in both lines with the red peak at the N_2H^+ velocity. The HCO^+ profile we see is symmetric (Figure 3).

SSV13 The Herbig-Haro objects HH 7-11 are excited by this source. Warin et al. (1996) have suggested that this source is triggering star formation in NGC 1333. Outflow wings are quite prominent in the CS, H_2CO (Mardones et al.) and HCO^+ profiles (Figure 4), but no significant skewness exists in the central core of the line.

NGC 1333 IRAS 2 Sandell et al. (1994) and Hodapp and Ladd (1995) observed two outflows, suggesting that this source may be a protobinary. Ward-Thompson et al. (1996) modeled the HCO^+ and $H^{13}CO^+$ $J = 4 - 3$ spectra as infall. Both the CS and H_2CO lines observed by Mardones et al. are skewed to the red. The HCO^+ $J = 3 - 2$ has the same self-absorption dip and blue-skewed profile as the $J = 4 - 3$ spectra (Figure 1).

IRAS03282+3035 Bachiller er al. (1991) observed a high velocity, well-collimated outflow in this source. Bachiller and Gomez-Gonzales (1992) identified this as an "extreme Class I" object, a category André et al. (1993) later called Class 0. The HCO^+ $J = 3 - 2$ has a slight blue asymmetry (Figure 3) but it is insufficient to qualify this source as a collapse candidate.

HH211 McCaughrean et al. (1994) discovered a molecular hydrogen jet with a dynamical age of less than 1000 years excited by a source detected only at wavelengths greater than 350 μm. Like the HCO^+ $J = 3 - 2$ spectra, the CS and H_2CO lines have no significant asymmetry (Mardones et al. 1997) (Figure 4).

IRAS04166+2706 Mardones et al. observed a symmetric line in H_2CO and a double-peaked line in CS with the stronger peak at the central velocity. The HCO^+ $J = 3 - 2$ line is nearly symmetric with a weak dip on the red-shifted side (Figure 1). The weaker of the two CS peaks lies within the blue HCO^+ line wing.

IRAS04169+2702 Ohashi et al. (1997) detected evidence for infall in a 2200 × 1100 AU envelope around this source using channel maps from interferometric observations of $C^{18}O$ $J = 1 - 0$. Mardones et al. saw outflow wings in CS. Our HCO^+ $J = 3 - 2$ data shows a symmetric profile (Figure 3), which encompasses the range of infall velocities seen by Ohashi et al., at the rest velocity of the source.

L1551 IRS5 The bipolar outflow was first seen in this source (Snell et al. 1980). Butner et al. (1991) found a density gradient consistent with the collapse model of Adams et al. (1987). Submillimeter interferometry revealed an 80 AU disk (Lay et al. 1994). Looney et al. (1997) interpreted their 2.7 mm interferometer observations as evidence that this source is a protobinary with each source separated by 50 AU (too small to be resolved by Lay et al.) and having a disk with a radius < 25 AU. Ohashi et al. (1996) observed in ^{13}CO $J = 2 - 1$ a much larger central condensation, 1200 by 670 AU, which had infalling motions. The H_2CO and CS lines (Mardones et al.), as well as our HCO^+ $J = 3 - 2$ line, are symmetric with outflow wings (Figure 3).

L1535 The H_2CO and CS observations of Mardones et al. show a symmetric line profile, as do our HCO^+ $J = 3 - 2$ data (Figure 3).

TMC-1A Wu et al. (1992) discovered a CO outflow in this source. CO $J = 1 - 0$ interferometer observations suggested the existence of a 2500 AU flattened structure (Tamura et al. 1996). Chandler et al. (1996) noted the similarity of the outflow to those of the Class 0 sources L1448-C and B335. Ohashi et al. (1997) measured a velocity gradient that would be expected from a rotating disk perpendicular to the outflow over a 580 AU radius. Mardones et al. observed symmetric lines in H_2CO and CS. The HCO^+ $J = 3 - 2$ line is double peaked with a stronger blue peak, but the N_2H^+ line of Mardones et al. (presumed to be optically thin) is near the red peak rather than between the two (Figure 1). The red peak of the HCO^+ $J = 3 - 2$ line is coincident with the peak of the CS line. There is no CS emission at the velocity of the blue peak, suggesting that the blue peak might be outflow emission.

L1634 A powerful molecular hydrogen jet is present in this source (Hodapp and Ladd 1995; Davis et al. 1997). The HCO^+ spectra has the blue peak slightly stronger than the red peak (Figure 1).

MMS1 This source and the following five were discovered by Chini et al. (1997), in the Orion high-mass star-forming region. Most of the other sources observed in this paper occur in low-mass star-forming regions. They were identified as Class 0 objects from their strong millimeter continuum emission. The HCO^+ $J = 3 - 2$ has a double-peaked profile with the red peak stronger (Figure 2).

MMS4 The red peak is slightly stronger than the blue peak in the HCO^+ $J = 3 - 2$ spectra (Figure 2).

MMS6 Little noticeable asymmetry is seen in the HCO^+ $J = 3 - 2$ spectra (Figure 3).

MMS9 The HCO^+ $J = 3 - 2$ line is symmetric (Figure 4).

MMS7 The HCO^+ $J = 3 - 2$ line has a slight red shoulder (Figure 4).

MMS8 This source has a highly collimated CO outflow (Chini et al. 1997). No asymmetry is observed in the HCO^+ $J = 3 - 2$ spectra (Figure 3).

NGC2264G Margulis and Lada (1986) discovered the molecular outflow which was later seen to be highly collimated and energetic (Margulis et al. 1988). Margulis et al. (1990) observed six near-infrared sources in this object, but Gomez et al. (1994) discovered the true driving source of the outflow, which was subsequently confirmed as a Class 0 object by Ward-Thompson et al. (1995). The HCO^+ $J = 3 - 2$ spectrum has a slight red wing (Figure 3).

B228 Heyer and Graham (1989) found evidence for a stellar wind from observations of extended [SiII] emission. Mardones et al. observed a slightly blue-skewed H_2CO line. The HCO^+ $J = 3 - 2$ line has a double peaked profile with a stronger blue peak like that predicted by collapse models (Figure 1). The $H^{13}CO^+$ $J = 3 - 2$ line is coincident with the red peak, but the N_2H^+ line peaks in the self-absorption dip of the HCO^+ line, suggesting that the $H^{13}CO^+$ line may be somewhat optically thick.

YLW16 The H_2CO has a prominent blue outflow shoulder (Mardones et al.). A similar feature appears in the HCO^+ $J = 3 - 2$ line (Figure 4).

L146 Clemens et al. (1998) identified this as a Class 0 or I source, an identification that corresponds well with its T_{bol} of 74 K. Mardones et al. observed a double-peaked line in CS and a blue-shouldered line in H_2CO. The HCO^+ $J = 3 - 2$ line is symmetric with a hint of a blue shoulder and agrees in velocity with the red peak in the CS spectrum (Figure 3).

S68N McMullin et al. (1994) first identified this core from CS and CH_3OH maps. Hurt and Barsony (1996) established this as a Class 0 source. Wolf-Chase et al. (1998) found an outflow flux consistent with those of other Class 0 sources. The CS and H_2CO lines show blue asymmetry with a prominent outflow shoulder (Mardones et al.). The HCO^+ $J = 3 - 2$ line has strong self-absorption with the red peak stronger than the blue peak. The red peak has the same velocity as the Mardones et al. spectra, while the blue peak has the same velocity as that of the CS profile. The $H^{13}CO^+$ line occurs at the same velocity as the self-absorption dip (Figure 2)

SMM6 This source is better known as SVS20 (Strom et al. 1976). The HCO^+ spectra is symmetric (Figure 4).

HH108 The Herbig-Haro objects, HH108 and HH109, are produced by a 9.5 $L_\odot$ IRAS source (Reipurth and Eiroa 1992). Reipurth et al. (1993) detected strong 1.3 mm emission. Both the CS $J = 2 - 1$ and H_2CO $J = 2_{12} - 1_{11}$ lines have peaks shifted to the red of the N_2H^+ velocity (Mardones et al.). Our HCO^+ line profile looks similar to that of the H_2CO $J = 2_{12} - 1_{11}$ line but with a slightly stronger blue peak (Figure 2).

CrA IRAS32 Both the H_2CO $J = 2_{12} - 1_{11}$ and CS $J = 2 - 1$ lines are symmetric (Mardones et al.). The HCO^+ $J = 3 - 2$ line has a double-peaked profile with a strong red peak and a dip near the velocity of the N_2H^+ line (Figure 2). The H_2CO and CS lines also peak in the HCO^+ dip.

L673A This core appears slightly elongated in continuum emission and is about 0.2 pc away from another core (Ladd et al. 1991). Like the H_2CO and CS spectra (Mardones et al.), the HCO^+ $J = 3 - 2$ line is symmetric (Figure 4).

L1152 The H_2CO $J = 2_{12} - 1_{11}$ and CS $J = 2 - 1$ lines are symmetric (Mardones et al.), as is the HCO^+ $J = 3 - 2$ line (Figure 4).

L1172 Submillimeter continuum maps of Ladd et al. (1991) showed extended emission at 100 and 160 μm. The CS $J = 2 - 1$ has a narrow self-absorption dip with the blue peak slightly stronger than the red peak (Mardones et al.). The HCO^+ spectrum (Figure 2) is slightly red-peaked and the two peaks agree in velocity with those in the CS spectrum (Mardones et al.). The N_2H^+ line has its peak in the HCO^+ self-absorption dip.

L1251A This source is located near the edge of its cloud and may be older than L1251B (Sato and Fukui 1989). The peak of the H_2CO line is slightly blue-shifted. The HCO^+ line is symmetric with prominent outflow wings (Figure 4).

L1251B Sato and Fukui (1989) discovered a molecular outflow in this source. Myers et al. (1996) matched a simple infall model to observed CS $J = 2 - 1$ and N_2H^+ $JF_1F = 101 - 012$ lines. The H_2CO $J = 2_{12} - 1_{11}$ line observed by Mardones et al. (1997) displays prominent self-absorption. The HCO^+ line profile is very strong with a prominent self-absorption dip and has the same velocity structure as the CS spectrum. The $H^{13}CO^+$ $J = 3 - 2$ line lies at the velocity of the dip, indicating that this may be a good candidate for protostellar collapse (Figure 1).

IRAS23011 Lefloch et al. (1996) identified this as a Class 0 source based on its millimeter continuum emission and its highly energetic outflow. Ladd and Hodapp (1997) observed a double outflow and measured a bolometric temperature of 61 K. The HCO^+ $J = 3 - 2$ has collapse asymmetry with the $H^{13}CO^+$ $J = 3 - 2$ lying between the two peaks (Figure 1).

CB244 Launhardt et al. (1997) identified this as a Class 0 object from its spectral energy distribution. The CS spectrum is symmetric, but the line is blue-shifted. The H_2CO $J = 2_{12} - 1_{11}$ line is blue-shifted with a prominent outflow wing. The HCO^+ $J = 3 - 2$ shows a blue-peaked line profile suggestive of collapse

(Figure 1). The N_2H^+ line observed by Mardones et al. is at the velocity of the self-absorption dip. The red peak in the HCO^+ $J = 3 - 2$ spectrum is at the same velocity as the H_2CO peak. The blue HCO^+ peak is at the same velocity as the CS line.

4. DISCUSSION

4.1. Line Profile Asymmetry

Models of a collapsing source with appropriate excitation requirements, a temperature and density gradient increasing toward the interior, predict that optically thick lines should show a double-peaked line profile with the blue-shifted peak stronger than the red-shifted peak and a self-absorption dip caused by the envelope at the rest velocity of the source (Leung and Brown 1977, Walker et al. 1986, Zhou 1992). The ratio of the peak temperatures of the blue and red peaks is a natural way to quantify this asymmetry, but this method requires lines that are double-peaked.

Since many of our line profiles are asymmetric without possessing two peaks, we also quantified the asymmetry using the asymmetry parameter defined in Mardones et al. as

$$\delta V = \frac{(V_{thick} - V_{thin})}{\Delta v_{thin}}$$

where V_{thick} is the velocity of the peak of the optically thick HCO^+ $J = 3 - 2$ line , V_{thin} is that of the optically thin line as determined by a Gaussian fit, and Δv_{thin} is the line width of the optically thin line. The optically thin line we used was $H^{13}CO^+$ $J = 3 - 2$ or, where that was not available, the N_2H^+ $JF_1F = 101 - 012$ line ($\nu = 93.176265$ GHz, Caselli et al. 1995) observed by Mardones et al. In Figure 5, we plot a histogram of the velocity of the $H^{13}CO^+$ line minus that of the N_2H^+ line. The mean velocity difference between the two lines is 0.15 ± 0.20 km s^{-1}. Following Mardones et al., we use δV of ± 0.25 as the threshold to be counted as either blue (if negative) or red (if positive). Also, we follow Mardones et al. in not considering an asymmetry as significant if the difference in strength between the blue and red peaks is less than twice the rms noise. For example, in L1634, the blue peak is only 0.11 K stronger than the red peak while the rms noise is 0.10 K; we do not consider this source to be an infall candidate. The results for δV are listed in Table 4 for the objects observed in this paper.

Among these sources, there are more blue than red objects. We can quantify this by using the blue excess, which is defined by Mardones et al. as

$$Blue\ Excess = \frac{N_{blue} - N_{red}}{N_{total}}.$$

If the blue line asymmetries expected from collapse are dominant in our sample, this will be a positive number. For the sources observed in this paper, the blue excess is 0.28.

4.2. Evolutionary Trends of the Line Profile

The sources observed in this paper can be combined with the 20 Class 0 and 3 Class I sources observed in Gregersen et al. (1997) to form a sample stretching from T_{bol} of 30 to 170 K, from the Class 0 stage well into the Class I stage. As in the previous section, we use for the optically thin line the $H^{13}CO^+$ $J = 3 - 2$

line when available and the N_2H^+ $JF_1F = 101 - 012$ line when it is not. The results for δV are plotted versus bolometric temperature in Figure 6.

For δV, there is no clear trend with bolometric temperature. We find a significant blue excess among both Class 0 and I sources. There is no dividing line past which the blue excess drops, a result markedly different from that of Mardones et al. who saw a disappearance of blue-skewed line profiles by the Class I stage. In fact, the blue peaked TMC-1A has the highest T_{bol}, 170 K, of any source in our sample. The results for δV for each class as well as for the combined sample are listed in Table 5.

To study the difference between lines, we plot δV as measured by the HCO^+ against those measured by the H_2CO and CS lines (Figure 7). The sources that appear in our blue excess and not those of Mardones et al. are in the box bounded by δV (H_2CO or CS) > -0.25 and $\delta V(HCO^+) < -0.25$. For example, TMC-1A and IRAS03235, sources with pronounced blue δV in HCO^+, show little asymmetry in CS and H_2CO. However, most of the differences between the tracers involve sources with no significant asymmetry in CS or H_2CO, but a significant one in HCO^+. Only a few sources have significant disagreements (upper left and lower right boxes outside the dashed lines in Figure 7). This pattern would be expected if the HCO^+ were more sensitive to infall in envelopes of lower opacity.

There are some sources that show markedly opposite asymmetries in CS or H_2CO as opposed to HCO^+. In the upper left corner of both plots, L1551-NE, a Class 0 source within an outflow lobe of L1551 IRS5, has a complicated HCO^+ $J = 3 - 2$ triple-peaked spectra (Gregersen et al.) with a very strong blue peak. The H_2CO and CS spectra are also triple-peaked, but the peaks are not so prominent that Mardones et al. were unable to fit a Gaussian to the line. We do not consider this source to be an infall candidate. Fitting a Gaussian in this case will give a redder velocity and thus a positive δV. In the lower right corner of the H_2CO-HCO^+ plot is L483, which has an H_2CO spectra with similar velocity structure but is blue-peaked in H_2CO and red-peaked in HCO^+.

Mardones et al. found good correlation between the CS and H_2CO δV (the two measures agree in 28 out of 38 instances) and Park et al. (1999) also found a good correlation between CS and the HCN $J = 1 - 0$ $F = 2 - 1$ line ($\nu = 88.631847$ GHz) and a fair correlation between H_2CO and HCN. We consider agreement as when both tracers are significantly blue or red or symmetric, disagreement as when one is significantly blue and the other significantly red and neutrality when one is significantly blue or red and the other is symmetric. CS and HCO^+ agree 13 times, are neutral 15 times and disagree 6 times. For H_2CO, there is agreement 16 times, neutrality 16 times and disagreement 5 times. For HCN, the asymmetries agree 7 times, are neutral 6 times and disagree 4 times.

4.3. An Evolutionary Model

Unlike the CS and H_2CO observations of Mardones et al., our HCO^+ observations of Class I sources do not show a radical change in the excess of sources with blue asymmetry at the Class 0-Class I boundary. Why do the HCO^+ results differ from those of HCN, CS and H_2CO? Perhaps infall asymmetry disappears at later times in HCO^+ than in HCN, CS and H_2CO.

For models in which the infall velocity increases closer to the forming star, each line of sight through the infall region intersects two points on the locus of constant radial velocity. To display infall asymmetry, a spectral line must be subthermally excited and fairly opaque at the foreground point of intersection. Different lines will be more suitable at different points in the evolution, as the density drops. Among the

lines in Table 6, the HCO^+ and H_2CO lines require the highest densities to excite (see Table 1 in Evans 1999) and HCO^+ has a higher opacity for typical abundances. Therefore, it is possible that the HCO^+ $J = 3 - 2$ line traces late stages of infall, when densities and opacities are lower, than the other lines.

To test this possibility and to study how the infall signature changes with time, one of the HCO^+ evolutionary models presented in Gregersen et al. has been extended to later times and collapse models have done for CS and H_2CO at those same times. The lines modeled are HCO^+ $J = 3 - 2$, CS $J = 2 - 1$ and H_2CO $J = 2_{12} - 1_{11}$, the lines observed by Gregersen et al. and Mardones et al., respectively. (The CS line has been modeled for early times by Zhou (1992) and Walker et al. (1994).) Protostellar collapse was simulated in a cloud with a radius of 0.2 pc using the velocity and density fields of the Shu (1977) collapse model and a temperature distribution scaled upward from that of B335 (Zhou et al. 1990) to a luminosity of 6.5 $L_\odot$, the average luminosity of the sources observed in Gregersen et al. Six models were run for infall radii of 0.005, 0.03, 0.06, 0.10, 0.13 and 0.16 pc, corresponding to infall times of 2.3×10^4 yr for the earliest model to 7.5×10^5 yr for the latest model. The cloud had 30 shells, 15 inside the infall radius and 15 outside. The model produces the velocity, density, kinetic temperature, turbulent width and molecular abundance for each shell. The same abundance (6×10^{-9}) was used for each molecule so these models would be the simplest possible comparisons of molecular tracers.

The output of the collapsing cloud simulation was used as input for a Monte Carlo code (Choi et al. 1995), which produces molecular populations in each shell. The output of the Monte Carlo code was used as input for a program that convolves a Gaussian beam with the emission from the cloud so we can simulate our HCO^+ CSO observations and the H_2CO IRAM and CS Haystack observations of Mardones et al. The distance to the model cloud was 310 pc, the average distance to the observed sources. The resulting line profiles are plotted in Figure 8.

The HCO^+ line profiles are the strongest and, at late times, the most asymmetric. The dashed horizontal line across each panel is the blue-red ratio. For CS and H_2CO, the blue-red ratio reaches a peak value and levels off, but the HCO^+ blue-red value keeps increasing. For all lines, the velocity of the blue-shifted peak becomes more negative with time from about -0.22 km s^{-1} to about -0.33 km s^{-1}. The profiles in Figure 8 support the conclusion that HCO^+ $J = 3 - 2$ reveals infall more readily than the CS and H_2CO lines. However, the model line profiles for those molecules predict a detectable signature as well. One possibility for obscuring the signature in other lines is that HCO^+ remains in the gas phase while the other species freeze out (Rawlings et al. 1992, Park et al. 1999).

One can question the relevance of our simulation, because none of the observed sources can be completely explained by the simple inside-out collapse model. For example, the simulated line profiles often have less extreme blue-red ratios than most of our infall candidates and the dip is much more extreme than in the observations. All of these sources are either turbulent, aspherical, or have very energetic bipolar outflows. Outflow is a large problem for HCO^+ $J = 3 - 2$ because emission from outflows is prominent in this line. Also, recent studies of pre-protostellar cores (e.g. Tafalla et al. 1999), cores seemingly in the earliest stages of collapse, have challenged the inside-out collapse model.

On the whole, the HCO^+ $J = 3 - 2$ line has both advantages and disadvantages in searching for infall. In the following section, we consider the information from all lines in assessing the best infall candidates.

4.4. New Infall Candidates?

Among the 34 sources observed here, we see 8 sources with the correct asymmetry for infall (Figure 1). (L1634 is eliminated from consideration for its weak asymmetry.) Three of these sources are Class 0, four are Class I and two are probably Class I. However, a blue-peaked optically thick line alone is not enough for a definite claim of infall.

For such a claim, the optically thin line must peak in the self-absorption dip of the optically thick line. We have observed the $H^{13}CO^+$ $J = 3 - 2$ line in 4 of our sources. In L1251B, NGC 1333 IRAS 2 and IRAS 23011, this condition is met. For sources where we did not observe the $H^{13}CO^+$ $J = 3 - 2$ line, we used the N_2H^+ $J = 1 - 0$ line of Mardones et al. to provide a rest velocity. Among the sources with blue peaks, N_2H^+ peaks in the dip of CB244, TMC-1A, IRAS 03235 and IRAS 04166, so we consider these to be good infall candidates. In B228, the N_2H^+ line is at the same velocity as the HCO^+ self-absorption dip, so we believe the $H^{13}CO^+$ $J = 3 - 2$ line may be optically thick in this source and we consider it to be a possible infall candidate. All the candidates that could have passed this test did so.

Since these sources have been observed in three optically thick lines, CS, H_2CO and HCO^+, with roughly comparable beamsizes, we can rank the worthiness of these sources as infall candidates (Table 6). Sources with a blue asymmetry in each of the three lines are the strongest infall candidates while those with blue asymmetries in two lines are the next strongest down to sources with one blue asymmetry. In each category, sources that display either blue or no asymmetry in each of the three lines are considered stronger candidates than those with red asymmetries. Sources above B228 are considered infall candidates. We include the HCN results of Park et al. for completeness, but consider them a secondary criteria since their beam was $1'$, larger than that in the observations of Gregersen et al. and Mardones et al.

Based on these criteria, L1251B is the strongest infall candidate of the sources studied here and is followed by CB244. Among the other six sources with infall asymmetry in HCO^+, NGC 1333 IRAS 2 has an H_2CO spectrum with a strong red peak and so is ruled out as an infall candidate since outflow seems likely as the explanation for the asymmetric profiles.

5. CONCLUSIONS

We have observed 16 Class I and 18 Class 0 sources in HCO^+ $J = 3 - 2$. Nine sources have a blue asymmetry and six have a red asymmetry. Infall asymmetries as defined by Mardones et al. are still present in Class I sources with $T_{bol} < 170$ K (blue excess = 0.31) to the same extent they are present among Class 0 sources with $T_{bol} < 70$ K (blue excess = 0.31). If the HCO^+ $J = 3 - 2$ line is more sensitive to infall, as evolutionary models suggest, than the CS and H_2CO lines studied by Mardones et al., then the end of the collapse phase still remains to be found. Among the sources we surveyed, we suggest six new infall candidates: CB 244, IRAS 03235, IRAS 04166, B228, IRAS23011 and TMC-1A. We confirm the suggestion of Myers et al. (1996) that L1251B is an infall candidates. NGC 1333 IRAS 2 is ruled out as an infall candidate, but has the weakest claim of any source studied here since it has blue asymmetry in HCO^+ and red asymmetry in H_2CO.

Although all the sources in this paper are young and protostellar, making an unambiguous claim for infall is somewhat difficult. If these sources are undergoing infall, then surely all of these sources should have blue asymmetries in every line. There is the optical depth effect previously mentioned where CS and H_2CO are optically thinner than HCO^+. However, there is also the problem that infall velocities are roughly

the same speed or less than turbulent and outflow motions. In the infall model previously presented, if such a source was observed with the resolution of our and Mardones et al.'s observations, at the radius of our beam, $\sim 25''$, for a source at 310 pc, infall speeds range from .07 km s^{-1} at the earliest times to 0.60 km s^{-1} at the latest stages. In real cores, for example, L1544, a pre-protostellar core probably at the beginning of the collapse phase, infall speeds are $\sim$ .1 km s^{-1}(Tafalla et al. 1999). Other caveats include beam size, the particular molecular transition chosen and the source mass. Detecting infall is a challenge.

For future work, we should observe CO to determine what velocity ranges are affected by outflows. Also, we should observe even later Class I sources to see if asymmetry is still common. Work is needed with higher spatial resolution to separate outflow from infall. Quantitative infall rates also need to be measured to see how the infall rate changes with time.

We would like to thank Daniel Jaffe, Wenbin Li, Kenji Mochizuki and Yancy Shirley for their help with observations. We would also like to thank Daniel Jaffe, John Lacy, Charles Lada and John Scalo for their comments on an early draft of this paper and the anonymous referee for helpful comments. This work was supported by NSF grant AST-9317567. D.M. thanks support from FONDECYT grant 1990632 and Fundacion Andes grant C-13413/7.

Table 1. List of Sources

Name	R.A. (1950.0)	Dec. (1950.0)	Offpos ($''$)	Distance (pc)	T_{bol} (K)
IRAS03235	03:23:33.0	30:04:59	(–1200,0)	350	<136
L1455	03:24:34.9	30:02:36	(–600,0)	350	67
IRAS03256	03:25:39.2	30:55:20	(–600,0)	350	<74
NGC 1333 IRAS 2	03:25:49.89	31:04:16.3	(0,–600)	350	52
SSV13	03:25:57.9	31:05:50	(–600,0)	350	136
IRAS03282	03:28:15.2	30:35:14	(–1200,0)	350	23
HH211	03:40:48.7	31:54:24	(–600,0)	350	30
IRAS04166	04:16:36.0	27:06:00	(–600,0)	140	91
IRAS04169	04:16:54.0	27:01:59	(–600,0)	140	170
L1551 IRS 5	04:28:40.2	18:01:42	(–600,0)	140	95
L1535	04:32:33.5	24:02:15	(–600,0)	140	61
TMC-1A	04:36:31.2	25:35:56	(–600,0)	140	170
L1634	05:17:21.9	-05:55:05	(0,-900)	415	77
MMS1	05:32:50.1	-05:02:13	(600,0)	415	>9
MMS4	05:32:52.6	-05:02:46	(600,0)	415	>9
MMS6	05:32:55.6	-05:03:25	(600,0)	415	>8
MMS9	05:32:58.2	-05:07:35	(600,0)	415	>9
MMS7	05:32:58.6	-05:05:46	(600,0)	415	96
MMS8	05:32:58.7	-05:07:10	(600,0)	415	>9
NGC2264G	06:38:25.76	09:58:52.41	(-600,0)	800	34
B228	15:39:50.4	-33:59:42	(0,–900)	150	48
YLW 16	16:24:26.2	-24:32:53	(0,–900)	125	157
L146	16:54:27.2	-16:04:48	(0,–900)	170	<56
S68N	18:27:15.5	01:14:50	(–900,0)	310	50
SMM6	18:27:25.4	01:12:02	(–900,0)	310	120
HH108	18:33:07.6	-00:35:48	(–900,0)	310	54
CrA IRAS32	18:59:35.8	-37:11:53	(0,–900)	130	148
L673A	19:18:04.6	11:14:12	(–900,0)	300	<55
L1152	20:35:19.4	67:42:30	(–900,0)	350	101
L1172	21:01:44.2	67:42:24	(–900,0)	350	44
L1251A	22:34:22.0	75:01:32	(–900,0)	300	<108
L1251B	22:37:40.8	74:55:50	(–900,0)	300	<91
IRAS23011	23:01:10.1	61:26:16	(-600,0)	730	57
CB244	23:23:48.7	74:01:08	(-900,0)	250	56

Note. — Class 0 sources have $T_{bol} < 70$ K and Class I sources have 70 K $\leq T_{bol} \leq$ 650 K. All bolometric temperatures are from Mardones et al. 1997 except for the following sources which were calculated using the following references: IRAS03282 (Barsony et al. 1998), L1535 (IRAS Point Source Catalog, Moriarty-Schieven et al. 1994), NGC2264G (Ward-Thompson et al. 1995), B228 (IRAS Point Source Catalog, Reipurth et al. 1993), L1634 (IRAS Point Source Catalog, Cohen et al. 1985, Reipurth et al. 1993), MMS1, MMS4, MMS6, MMS9, MMS7, MMS8 (Chini et al. 1997), S68N (Hurt and Barsony 1996, Wolf-Chase et al. 1998), SMM6 (Hurt and Barsony 1996, Casali et al. 1993), L1152 (Myers et al. 1987, IRAS Point Source Catalog), L1172 (IRAS Point Source Catalog, Ladd et al. 1991), IRAS23011 (IRAS Point Source Catalog, Lefloch et al. 1996) and CB244 (IRAS Point Source Catalog, Launhardt et al. 1997).

Table 2. List of Observed Lines

Molecule	Transition	Beamwidth ($''$)	η_{mb}	δv (km s^{-1})	Frequency (GHz)
$H^{13}CO^+$	$J = 3 - 2$	26	0.66	0.11	260.255478
HCO^+	$J = 3 - 2$	26	0.66	0.11	267.557620

Table 3. Results

Source	Line	T_A^* (K)	Velocity (km s^{-1})	ΔV (km s^{-1})
IRAS03235	HCO^+ $J = 3 - 2$	0.87±0.04	4.91±0.06	1.09±0.12
–	–	0.42±0.04	5.64±0.06	–
L1455	HCO^+ $J = 3 - 2$	2.65±0.10	4.29±0.06	1.33±0.12
IRAS03256	HCO^+ $J = 3 - 2$	1.38±0.10	7.27±0.02	0.91±0.06
NGC 1333 IRAS 2	$H^{13}CO^+$ $J = 3 - 2$	1.07±0.06	7.68±0.02	1.04±0.04
–	HCO^+ $J = 3 - 2$	2.33±0.06	7.07±0.07	2.85±0.14
–	–	1.72±0.06	8.64±0.07	–
SSV13	HCO^+ $J = 3 - 2$	3.87±0.10	8.37±0.01	2.07±0.03
IRAS03282	$H^{13}CO^+$ $J = 3 - 2$	0.21±0.04	7.13±0.04	0.65±0.12
–	HCO^+ $J = 3 - 2$	2.12±0.03	6.79±0.08	0.95±0.16
HH211	HCO^+ $J = 3 - 2$	2.41±0.06	9.24±0.08	1.16±0.15
IRAS04166	HCO^+ $J = 3 - 2$	1.33±0.04	6.35±0.06	1.94±0.12
–	–	0.51±0.04	7.07±0.06	–
IRAS04169	HCO^+ $J = 3 - 2$	0.99±0.07	6.93±0.01	0.61±0.04
L1551 IRS5	HCO^+ $J = 3 - 2$	6.11±0.10	6.58±0.01	1.14±0.01
L1535	HCO^+ $J = 3 - 2$	1.32±0.06	5.43±0.01	0.78±0.02
TMC-1A	HCO^+ $J = 3 - 2$	1.27±0.04	5.97±0.06	1.45±0.12
–	–	1.04±0.04	6.58±0.06	–
L1634	HCO^+ $J = 3 - 2$	2.22±0.10	7.80±0.07	1.14±0.13
–	–	2.11±0.10	8.51±0.07	–
MMS1	HCO^+ $J = 3 - 2$	3.47±0.09	10.48±0.06	2.18±0.12
–	–	4.53±0.09	11.69±0.06	–
MMS4	HCO^+ $J = 3 - 2$	3.74±0.09	10.80±0.06	1.69±0.12
–	–	4.28±0.09	11.45±0.06	–
MMS6	HCO^+ $J = 3 - 2$	6.30±0.09	11.08±0.01	1.83±0.01
MMS9	HCO^+ $J = 3 - 2$	4.99±0.10	11.49±0.01	1.70±0.02
MMS7	HCO^+ $J = 3 - 2$	3.35±0.10	10.56±0.01	1.85±0.02
MMS8	HCO^+ $J = 3 - 2$	5.05±0.11	11.49±0.01	1.18±0.02
NGC2264G	$H^{13}CO^+$ $J = 3 - 2$	0.18±0.04	4.56±0.06	0.74±0.12
–	HCO^+ $J = 3 - 2$	1.24±0.03	4.57±0.01	1.28±0.03
B228	$H^{13}CO^+$ $J = 3 - 2$	0.57±0.04	5.38±0.01	0.57±0.03
–	HCO^+ $J = 3 - 2$	2.58±0.04	4.96±0.05	1.09±0.11
–	–	1.84±0.04	5.51±0.05	–
YLW 16	HCO^+ $J = 3 - 2$	0.90±0.10	4.51±0.05	2.18±0.11
L146	HCO^+ $J = 3 - 2$	2.77±0.13	5.36±0.01	0.55±0.03
S68N	$H^{13}CO^+$ $J = 3 - 2$	0.81±0.10	8.83±0.03	1.30±0.08
–	HCO^+ $J = 3 - 2$	2.35±0.09	7.22±0.06	4.35±0.12
–	–	3.87±0.09	9.57±0.06	–
SMM6	HCO^+ $J = 3 - 2$	4.51±0.11	1.91±0.03	7.69±0.01
HH108	HCO^+ $J = 3 - 2$	1.13±0.03	10.38±0.06	1.36±0.12
–	–	1.75±0.03	11.00±0.06	–
CrA IRAS32	HCO^+ $J = 3 - 2$	1.32±0.04	5.08±0.06	1.61±0.12
–	–	2.27±0.04	5.95±0.06	–
L673A	HCO^+ $J = 3 - 2$	2.46±0.09	6.92±0.01	1.05±0.02
L1152	HCO^+ $J = 3 - 2$	2.43±0.11	2.45±0.01	0.68±0.02
L1172	$H^{13}CO^+$ $J = 3 - 2$	<0.05	–	–
–	HCO^+ $J = 3 - 2$	1.08±0.03	2.54±0.06	1.12±0.12
–	–	1.14±0.03	3.16±0.06	–
L1251A	HCO^+ $J = 3 - 2$	2.10±0.10	-4.91±0.02	2.39±0.05
L1251B	$H^{13}CO^+$ $J = 3 - 2$	0.69±0.06	-3.70±0.02	1.12±0.05
–	HCO^+ $J = 3 - 2$	4.50±0.04	-4.34±0.06	2.11±0.12
–	–	3.21±0.04	-2.98±0.06	–
IRAS23011	$H^{13}CO^+$ $J = 3 - 2$	0.50±0.06	-11.04±0.05	1.31±0.13
–	HCO^+ $J = 3 - 2$	2.82±0.06	-11.58±0.07	3.18±0.14
–	–	1.81±0.06	-10.57±0.07	–
CB244	HCO^+ $J = 3 - 2$	2.73±0.04	3.75±0.06	1.61±0.12
–	–	1.80±0.04	4.62±0.06	–

Table 4. Line Asymmetries

Source	Asymmetry	Blue/Red
IRAS03235	-0.66±0.18	2.07
L1455	-0.71±0.09	-
IRAS03256	-0.35±0.07	-
NGC 1333 IRAS 2	-0.59±0.11	1.35
SSV13	-0.11±0.02	-
IRAS03282	-0.52±0.17	-
HH211	0.31±0.18	–
IRAS04166	-0.97±0.18	2.61
IRAS04169	0.07±0.05	-
L1551 IRS 5	0.20±0.02	-
L1535	-0.60±0.04	-
TMC-1A	-1.02±0.15	1.22
L1634	-	1.06
MMS1	-	0.77
MMS4	-	0.87
MMS6	-	-
MMS9	-	-
MMS7	-	-
MMS8	-	-
NGC2264G	0.01±0.08	
B228	-0.74±0.10	1.40
YLW 16	0.45±0.07	-
L146	0.40±0.14	-
S68N	0.57±0.07	0.74
SMM6	-	-
HH108	0.29±0.09	0.65
CrA IRAS32	0.48±0.12	0.58
L673A	0.00±0.04	-
L1152	-0.63±0.06	-
L1172	0.72±0.12	0.95
L1251A	0.16±0.05	-
L1251B	-0.57±0.06	1.40
IRAS23011	-0.41±0.08	1.55
CB244	-1.02±0.14	1.52

Table 5. Asymmetries – Overall Sample

Class	N	Blue	Neither	Red	Blue Excess
0	26	15	4	7	0.31
I	16	8	5	3	0.31
Overall	42	23	9	10	0.31

Table 6. Asymmetries by source

Source	CS	H_2CO	HCO^+	HCN
NGC 1333 IRAS 4A	B	B	B	B
L1157	B	B	B	B
L1251B	B	B	B	B
NGC 1333 IRAS 4B	B	B	B	-
IRAS16293	B	B	B	-
L483	B	B	R	B
B335	B	B	B	R
IRAS03256	B	N	B	-
L1527	N	B	B	-
Serpens SMM4	N	B	B	N
CB244	B	N	B	N
L483	B	B	R	B
VLA1623	B	B	R	N
S68N	B	B	R	-
IRAS03235	N	N	B	-
IRAS03282	N	N	B	-
IRAS04166	N	N	B	-
L1535	N	N	B	-
L1152	N	N	B	N
TMC-1A	N	N	B	-
L1455	-	N	B	-
B228	-	N	B	-
NGC 1333 IRAS 2	N	R	B	N
L1251A	R	B	N	N
L1172	-	N	R	B
L1448-N	N	N	N	N
SSV13	N	N	N	-
IRAS04169	N	N	N	-
L723	N	N	N	-
L673A	N	N	N	N
HH211	N	N	R	-
L1551	R	N	N	-
L146	N	N	R	R
HH108	N	N	R	N
CrA IRAS32	N	N	R	-
L146	N	N	R	R
L1172	-	N	R	B
L1448-C	B	R	R	B
L1551-NE	R	R	B	-
Serpens SMM1	B	R	R	-

REFERENCES

Adams, F. C., Lada, C. J., & Shu, F. H. 1987, ApJ, 312, 788

André, P., Ward-Thompson, D., & Barsony, M. 1993, ApJ, 406, 122

Bachiller, R. & Gomez-Gonzales, J. 1992, A&AReview, 3, 257

Bachiller, R., Martin-Pintado, J., & Planesas, P. 1991, A&A, 251, 639

Barsony, M., Ward-Thompson, D., André, P., & O'Linger, J. 1998, ApJ, 509, 733

Butner, H. M., Evans, N. J., II, Lester, D. F., Levreault, R. M., & Strom, S. E. 1991, ApJ, 376, 636

Casali, M. M., Eiroa, C., & Duncan, W. D. 1993, A&A, 275, 195

Caselli, P., Myers, P. C., & Thaddeus, P. 1995, ApJ, 455, L77

Chandler, C. J., Terebey, S., Barsony, M., Moore, T. J. T., & Gautier, T. N. 1996, ApJ, 471, 308

Chini, R., Reipurth, B., Ward-Thompson, D., Bally, J., Nyman, L.-A., Sievers, A., & Billawala, Y. 1997, ApJ, 474, L135

Choi, M., Evans, N. J., II, Gregersen, E. M., & Wang, Y. 1995, ApJ, 448, 742

Clemens, D., Byrne, A., Yun, J. L., & Kane, B. 1998, in ASP Conf. Ser. 132, Star Formation with the Infrared Space Observatory, ed. J. Yun & R. Liseau (San Francisco: ASP), 334

Cohen, M., Harvey, P. M., & Schwartz, R. D. 1985, ApJ, 296, 633

Davidson, J. A. & Jaffe, D. T. 1984, ApJ, 277, L13

Davis, C. J., Ray, T. P., Eisloffel, J., & Corcoran, D. 1997, A&A, 324, 263

Evans, N. J., II 1999 Annu. Rev. Astr. Ap. 37, in press

Frerking, M. A. & Langer, W. D. 1982, ApJ, 256, 523

Goldsmith, P. F., Snell, R. L., Hemeon-Heyer, M., & Langer, W. D. 1984, ApJ, 286, 599

Gomez, J. F., Curiel, S., Torrelles, J. M., Rodriguez, L. F., Anglada, G., & Girart, J. M. 1994, ApJ, 436, 749

Gregersen, E. M., Evans, N. J., II, Zhou, S., & Choi, M. 1997, ApJ, 484, 256

Heyer, M. H. & Graham, J. A. 1989, PASP, 101, 816

Hodapp, K.-W. & Ladd, E. F. 1995, ApJ, 453, 715

Hughes, J. D., Hartigan, P., Krautter, J., & Kelemen, J., 1994, AJ, 108, 1071

Hurt, R. L. & Barsony, M. 1996, ApJ, 460, L45

Hurt, R. L., Barsony, M. & Wootten, A. 1996, ApJ, 456, 686

Kooi, J. W., Chan, M., Phillips, T. G., Bumble, B., & LeDuc, H. G. 1992, IEEE Transactions on Microwave Theory and Techniques, 40, 812

Ladd, E. F., Adams, F. C., Casey, S., Davidson, J. A., Fuller, G. A., Harper, D. A., Myers, P. C., & Padman, R. 1991, ApJ, 382, 555

Ladd, E. F. & Hodapp, K.-W. 1997, ApJ, 474, 749

Ladd, E. F., Lada, E. A., & Myers, P. C. 1993, ApJ, 410, 168

Launhardt, R., Ward-Thompson, D., & Henning, T. 1997, MNRAS, 288, L45

Lay, O. P., Carlstrom, J. E., Hills, R. E., & Phillips, T. G. 1994, ApJ, 434, L75

Lefloch, B., Eisloffel, J., & Lazareff, B. 1996, A&A, 313, L17

Lehtinen, K. 1997, A&A, 317, L5

Leung, C. M. & Brown, R. L. 1977, ApJ, 214, L73

Looney, L. W., Mundy, L. G., & Welch, W. J. 1997, ApJ, 484, L157

Mardones, D., Myers, P. C., Tafalla, M., Wilner, D. J., Bachiller, R., & Garay, G. 1997, ApJ, 489, 719

Margulis, M. & Lada, C. J. 1986, ApJ, 309, L87

Margulis, M., Lada, C. J., Hasegawa, T., Hayashi, S. S., Hayashi, M., Kaifu, N., Gatley, I., Greene, T. P., & Young, E. T. 1990, ApJ, 352, 615

Margulis, M., Lada, C. J., & Snell, R. L. 1988, ApJ, 333, 316

McCaughrean, M. J., Rayner, J. T., & Zinnecker, H. 1994, ApJ, 436, L189

McMullin, J. P., Mundy, L. G., Wilking, B. A., Hezel, T., & Blake, G. A. 1994, ApJ, 424, 222

Moriarty-Schieven, G. H., Wannier, P. G., Magnum, J. G., Tamura, M., & Olmsted, V. K. 1995, ApJ, 455, 190

Moriarty-Schieven, G. H., Wannier, Keene, J., & Tamura, M. 1994, ApJ, 436, 800

Myers, P. C., Fuller, G. A., Mathieu, R. D., Beichman, C. A., Benson, P. J., Schild, R. E., & Emerson, J. P. 1987, ApJ, 319, 340

Myers, P. C. & Ladd, E. F. 1993, ApJ, 413, L47

Myers, P. C., Mardones, D., Tafalla, M., Williams, J. P., & Wilner, D. J. 1996, ApJ, 465, L133

Ohashi, N., Hayashi, M., Ho, P. T. P., Momose, M., Tamura, M., & Hirano, N. 1996, ApJ, 466, 957

Ohashi, N., Hayashi, M., Ho, P. T. P., Momose, M., Tamura, M., Hirano, N., & Sargent, A. I. 1997, ApJ, 488, 317

Park, Y.-S., Kim, J., & Minh, Y. C., 1999, ApJ, 520, 223

Rawlings, J. M. C., Hartquist, T. W., Menten, K. M., & Williams, D. A. 1992, MNRAS, 255, 471

Reipurth, B., Chini, R., Krugel, E., Kreysa, E., & Sievers, A. 1993, A&A, 273, 221

Reipurth, B. & Eiroa, C. 1992, A&A, 256, L1

Sandell, G., Knee, L. B. G., Aspin, C., Robson, I. E., & Russell, A. P. G. 1994, A&A, 285, L1

Sato, F. & Fukui, Y. 1989, ApJ, 343, 773

Shu, F. H. 1977, ApJ, 214, 488

Snell, R. L., Loren, R. B., & Plambeck, R. L. 1980, ApJ, 239, L17

Strom, S. E., Vrba, F. J., & Strom, K. M. 1976, AJ, 81, 638

Tamura, M., Ohashi, N., Hirano, N., Itoh, Y., & Moriarty-Schieven, G. H. 1996, AJ, 112, 2076

Walker, C. K., Lada, C. J., Young, E. T., Maloney, P. R., & Wilking, B. A. 1986, ApJ, 309, L47

Walker, C. K., Narayanan, G., & Boss, A. P. 1994, ApJ, 431, 767

Ward-Thompson, D., Buckley, H. D., Greaves, J. S., Holland, W. S., & André, P. 1996, MNRAS, 281, L53

Ward-Thompson, D., Eiroa, C., & Casali, M. M. 1995, MNRAS, 273, L25

Warin, S., Castets, A., Langer, W. D., Wilson, R. W., & Pagani, L. 1996, A&A, 306, 935

Wolf-Chase, G. A., Barsony, M., Wootten, H. A., Ward-Thompson, D., Lowrance, P. J., Kastner, J. H., & McMullin, J. P. 1998, ApJ, 501, L193

Wu, Y., Zhou, S., & Evans, N. J., II 1992, ApJ, 394, 196

Yun, J. L. & Clemens, D. P. 1995, AJ, 109, 742

Zhou, S. 1992, ApJ, 394, 204

Zhou, S., Evans, N. J., II, Butner, H. M., Kutner, M. L., Leung, C. M., & Mundy, L. G. 1990, ApJ, 363, 168

Zhou, S., Evans, N. J., II, Kompe, C., & Walmsley, C. M. 1993, ApJ, 404, 232

Zhou, S., Evans, N. J., II, Wang, Y., Peng, R., & Lo, K. Y. 1994, ApJ, 433, 131

Fig. 1.— HCO^+ and $H^{13}CO^+$ $J = 3 - 2$ spectra toward the center of five Class 1 sources and four Class 0 sources. These sources all show a blue asymmetry in the HCO^+ $J = 3 - 2$ line characteristic of collapse. The solid line is the HCO^+ spectrum and the dashed line is the $H^{13}CO^+$ spectrum. The dashed vertical line is the velocity of the N_2H^+ $J = 1 - 0$ line observed by Mardones et al. The intensity and velocity scales for the L1251B spectra are shown on the right and top side of its panel, respectively. The velocity scale for the IRAS23011 spectra is the same as that of L1251B.

Fig. 2.— HCO^+ and $H^{13}CO^+$ $J = 3 - 2$ spectra toward the center of one Class 1 and five Class 0 sources that all show a red asymmetry in the HCO^+ $J = 3 - 2$ line. The solid line is the HCO^+ spectrum and the dashed line is the $H^{13}CO^+$ spectrum. The dashed vertical line is the velocity of the N_2H^+ $J = 1 - 0$ line observed by Mardones et al.

Fig. 3.— HCO^+ $J = 3 - 2$ spectra toward the center of three Class I sources and seven Class 0 sources that do not show any clear asymmetry in the HCO^+ $J = 3 - 2$ line. The solid line is the HCO^+ spectrum and the dashed line is the $H^{13}CO^+$ spectrum. The dashed vertical line is the velocity of the N_2H^+ $J = 1 - 0$ line observed by Mardones et al.

Fig. 4.— HCO^+ $J = 3 - 2$ spectra toward the center of six Class I and three Class 0 sources that do not show any clear asymmetry in the HCO^+ $J = 3 - 2$ line. The dashed vertical line is the velocity of the N_2H^+ $J = 1 - 0$ line observed by Mardones et al. The velocity scale for the L1251A spectra is shown on the top side of its panel.

Fig. 5.— Histogram of the velocity of the $H^{13}CO^+$ $J = 3 - 2$ line minus that of the N_2H^+ $J = 101 - 012$ line.

Fig. 6.— The δv of the observed line profiles vs. bolometric temperature.

Fig. 7.— The top panel is the δv of the HCO^+ $J = 3 - 2$ line profile vs. that of the CS $J = 2 - 1$ line. The bottom panel is the δv of the HCO^+ $J = 3 - 2$ line profile vs. that of the H_2CO $J = 2_{12} - 1_{11}$ line.

Fig. 8.— The top row is a set of six models following the temporal evolution of the HCO^+ $J = 3 - 2$ line profile. The middle row follows the evolution of the H_2CO $J = 2_{12} - 1_{11}$ line profile. The bottom row follows the evolution of the CS $J = 2 - 1$ line profile. The intensity scale is in T_A^*. The dashed horizontal lines are the blue-red ratios.

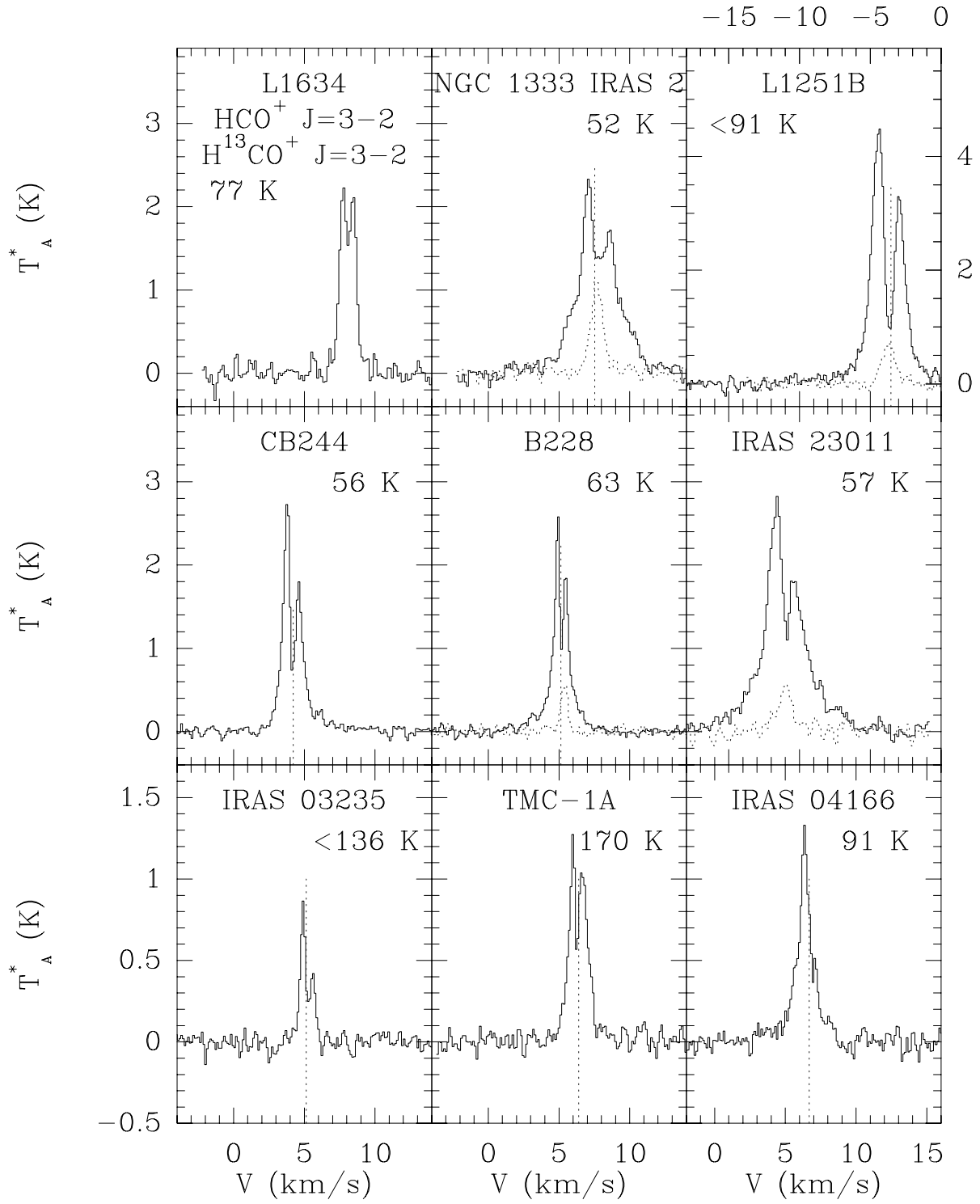
L1634
HCO+ J=3−2
H13CO+ J=3−2
77 K
NGC 1333 IRAS 2
52 K
L1251B
<91 K
CB244
56 K
B228
63 K
IRAS 23011
57 K
IRAS 03235
<136 K
TMC−1A
170 K
IRAS 04166
91 K
T*A (K)
V (km/s)

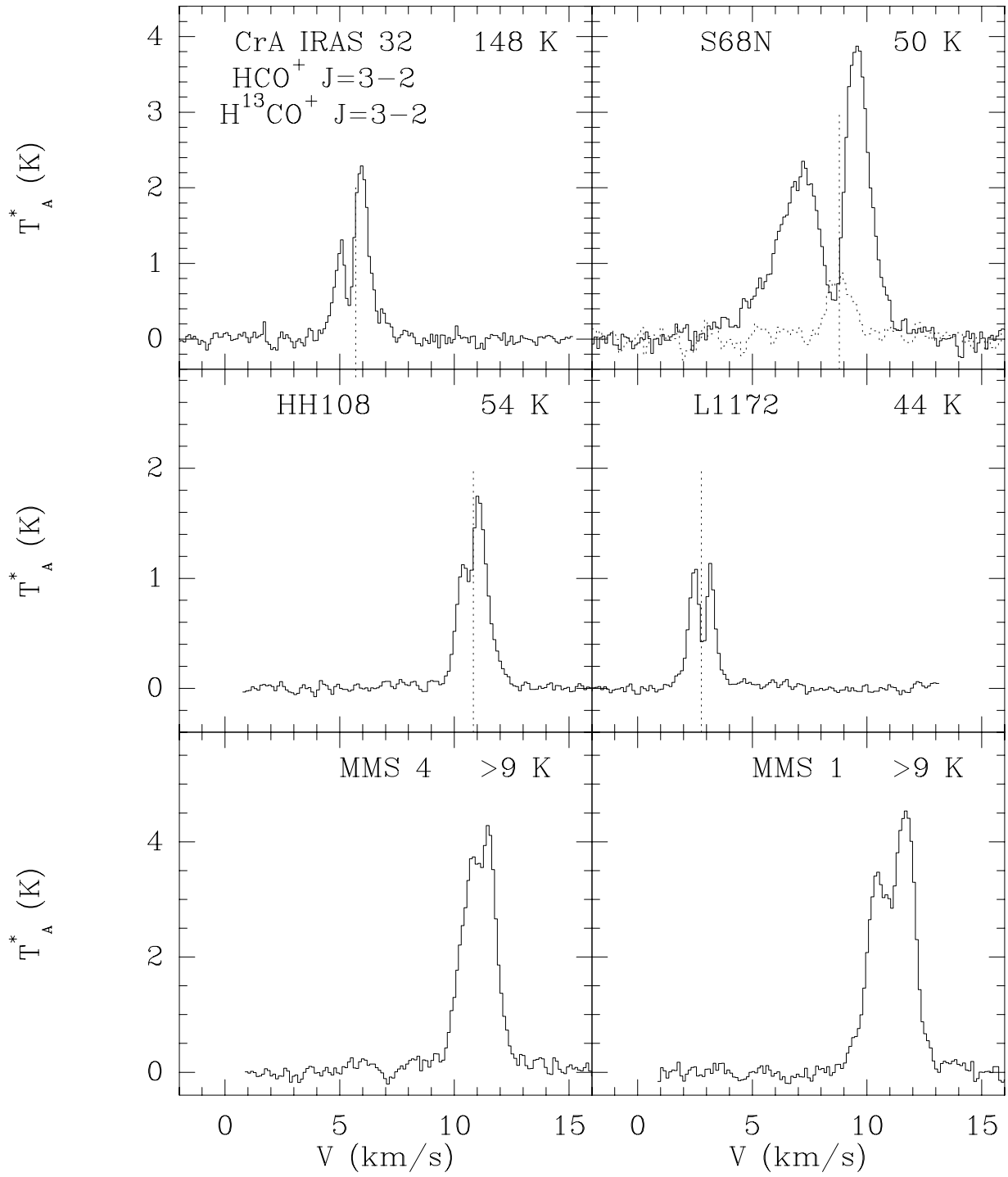
CrA IRAS 32 148 K
HCO+ J=3−2
H13CO+ J=3−2
S68N 50 K
HH108 54 K
L1172 44 K
MMS 4 >9 K
MMS 1 >9 K
T*A (K)
V (km/s)

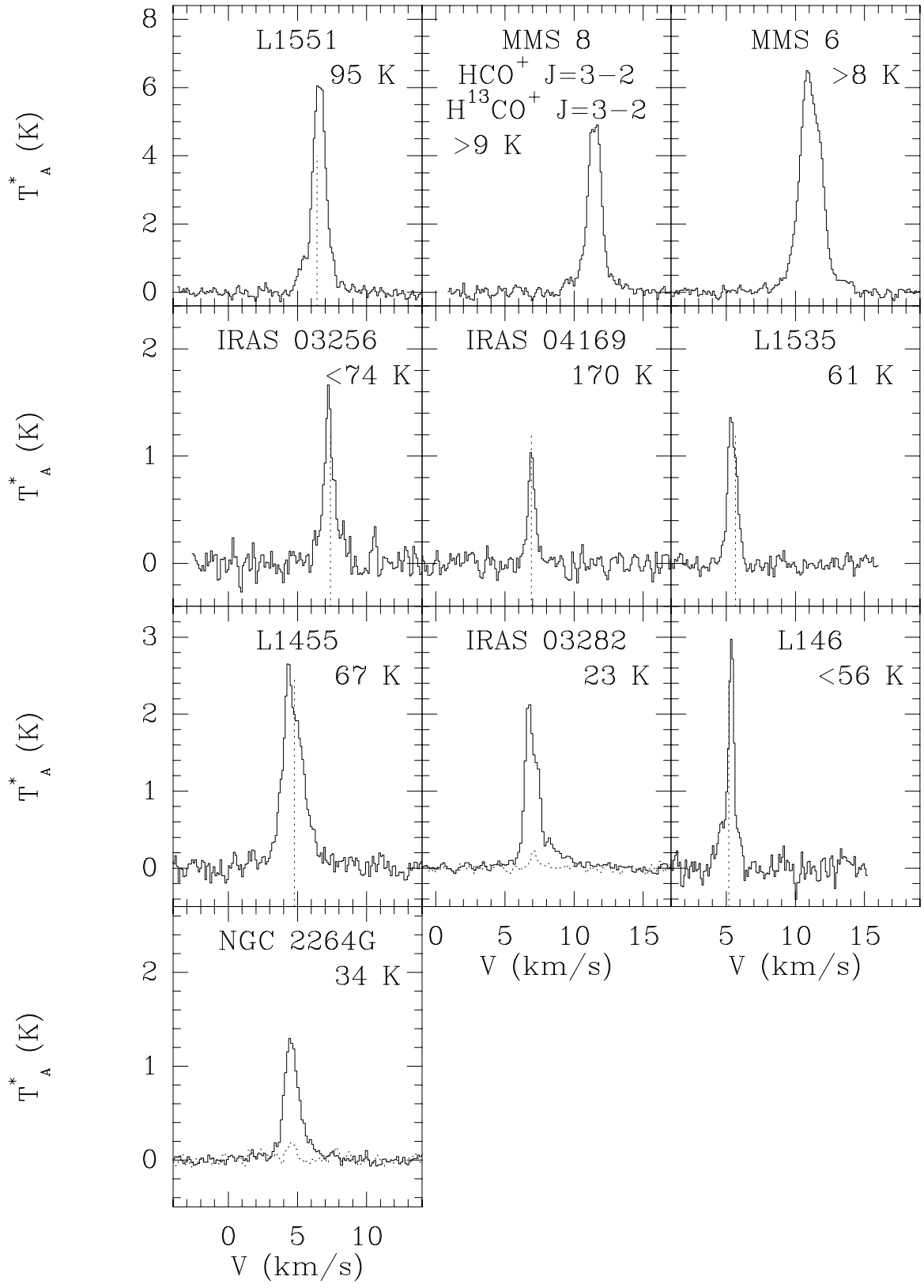
L1551
95 K
MMS 8
HCO+ J=3−2
H13CO+ J=3−2
>9 K
MMS 6
>8 K
IRAS 03256
<74 K
IRAS 04169
170 K
L1535
61 K
L1455
67 K
IRAS 03282
23 K
L146
<56 K
NGC 2264G
34 K
T*A (K)
V (km/s)

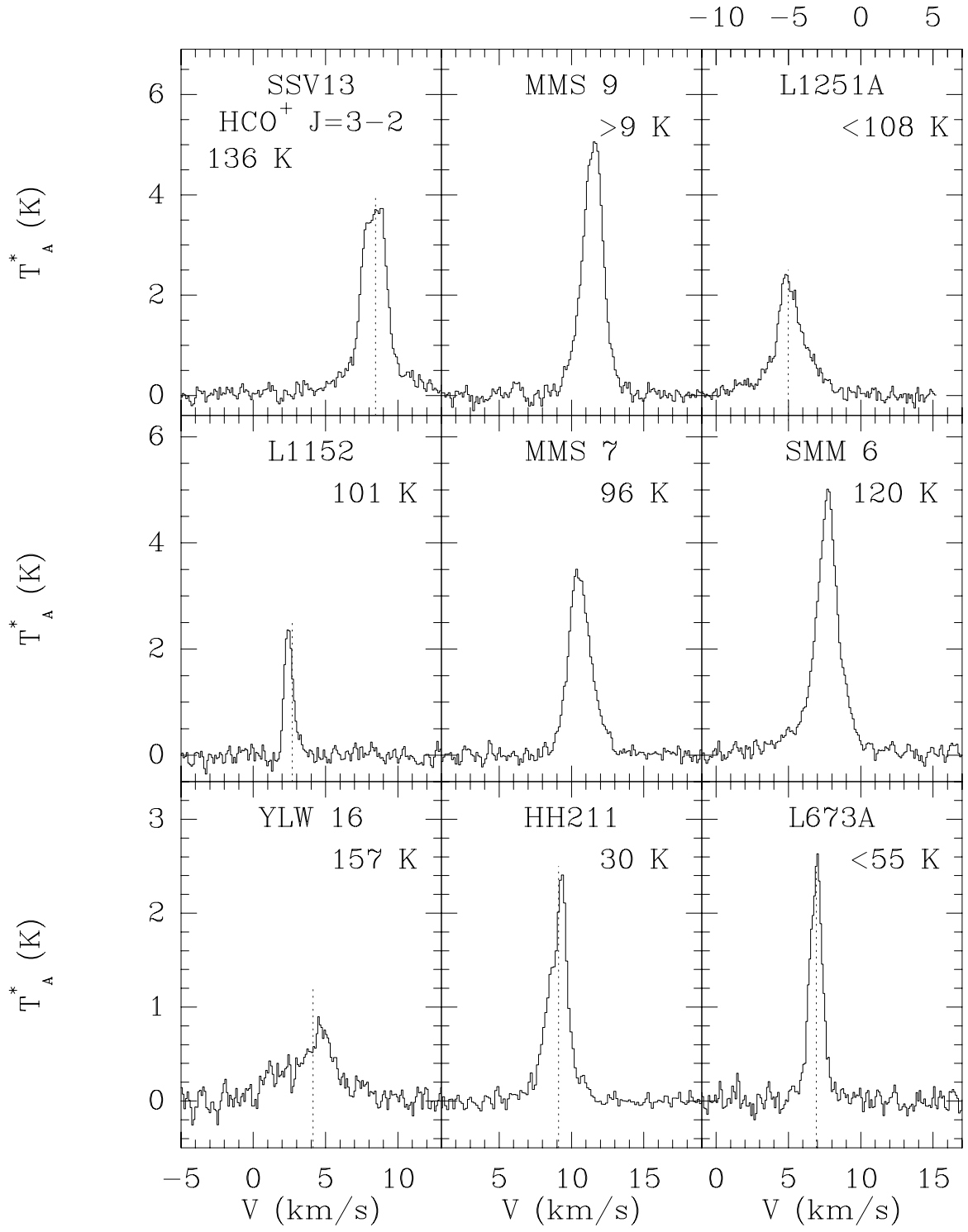
SSV13
HCO+ J=3−2
136 K
MMS 9
>9 K
L1251A
<108 K
L1152
101 K
MMS 7
96 K
SMM 6
120 K
YLW 16
157 K
HH211
30 K
L673A
<55 K
T*A (K)
V (km/s)

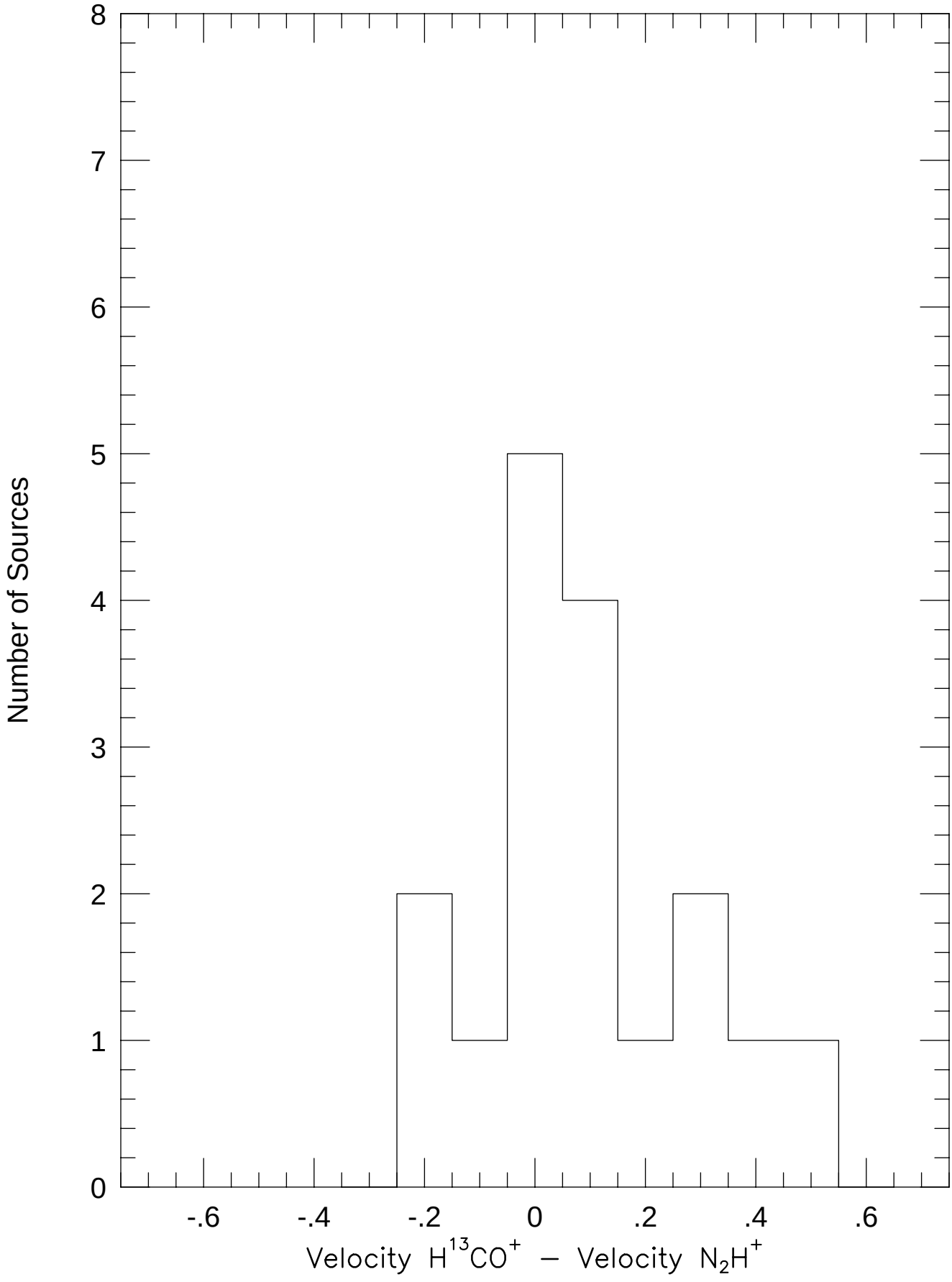
Number of Sources
0
1
2
3
4
5
6
7
8
-.6
-.4
-.2
0
.2
.4
.6
Velocity $H^{13}CO^+$ – Velocity N_2H^+

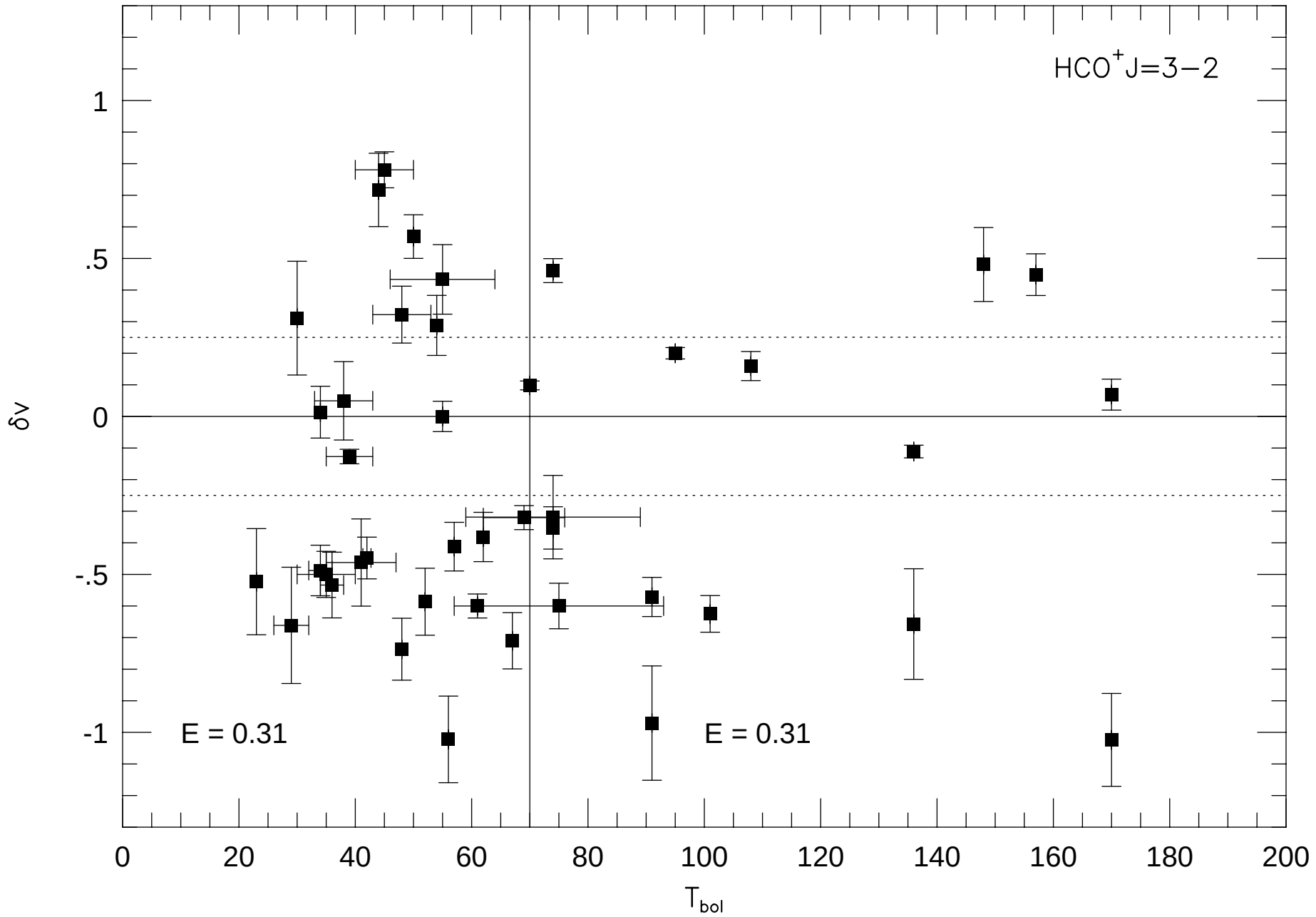
HCO+J=3−2
δv
1
.5
0
-.5
-1
E = 0.31
E = 0.31
0
20
40
60
80
100
120
140
160
180
200
Tbol

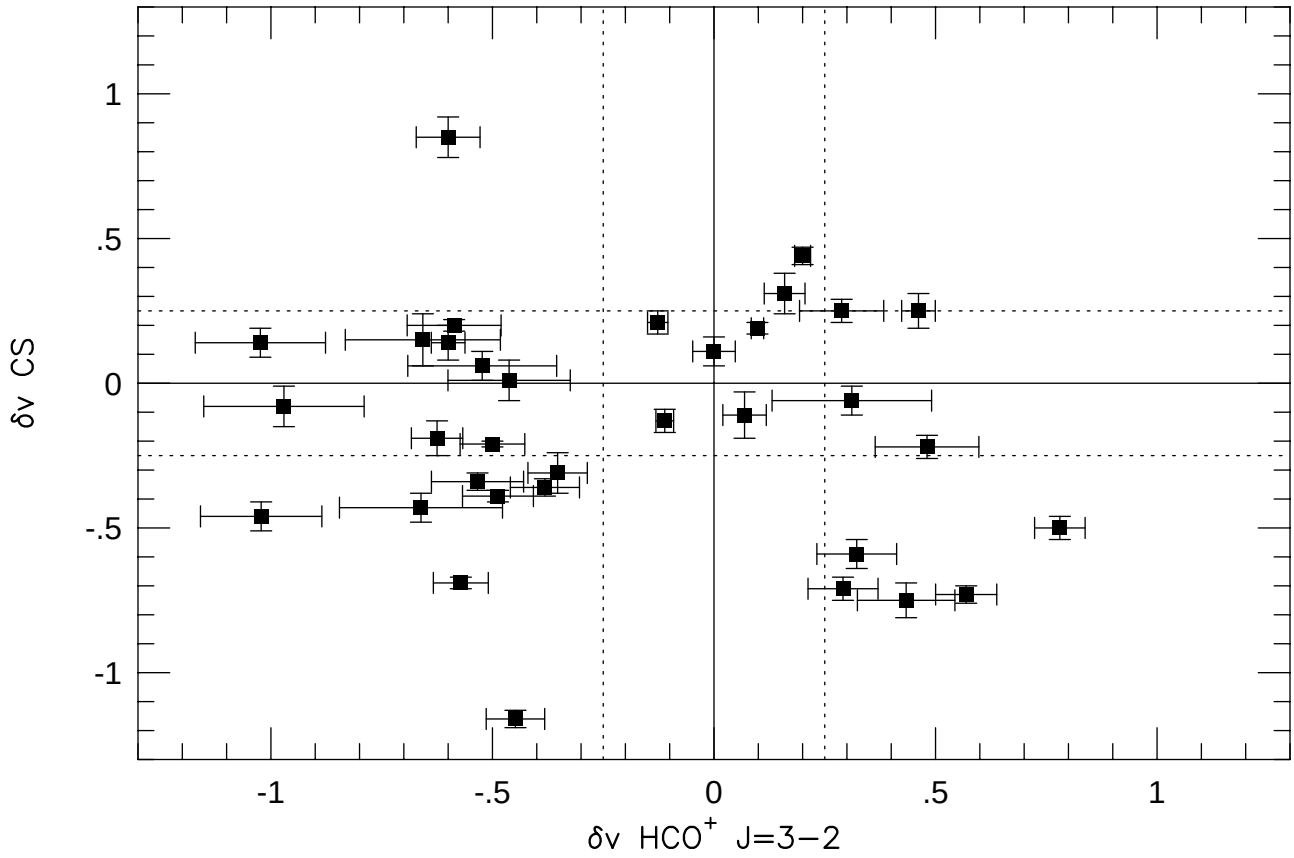
1
.5
0
-.5
-1
δv CS
-1
-.5
0
.5
1
δv HCO+ J=3−2

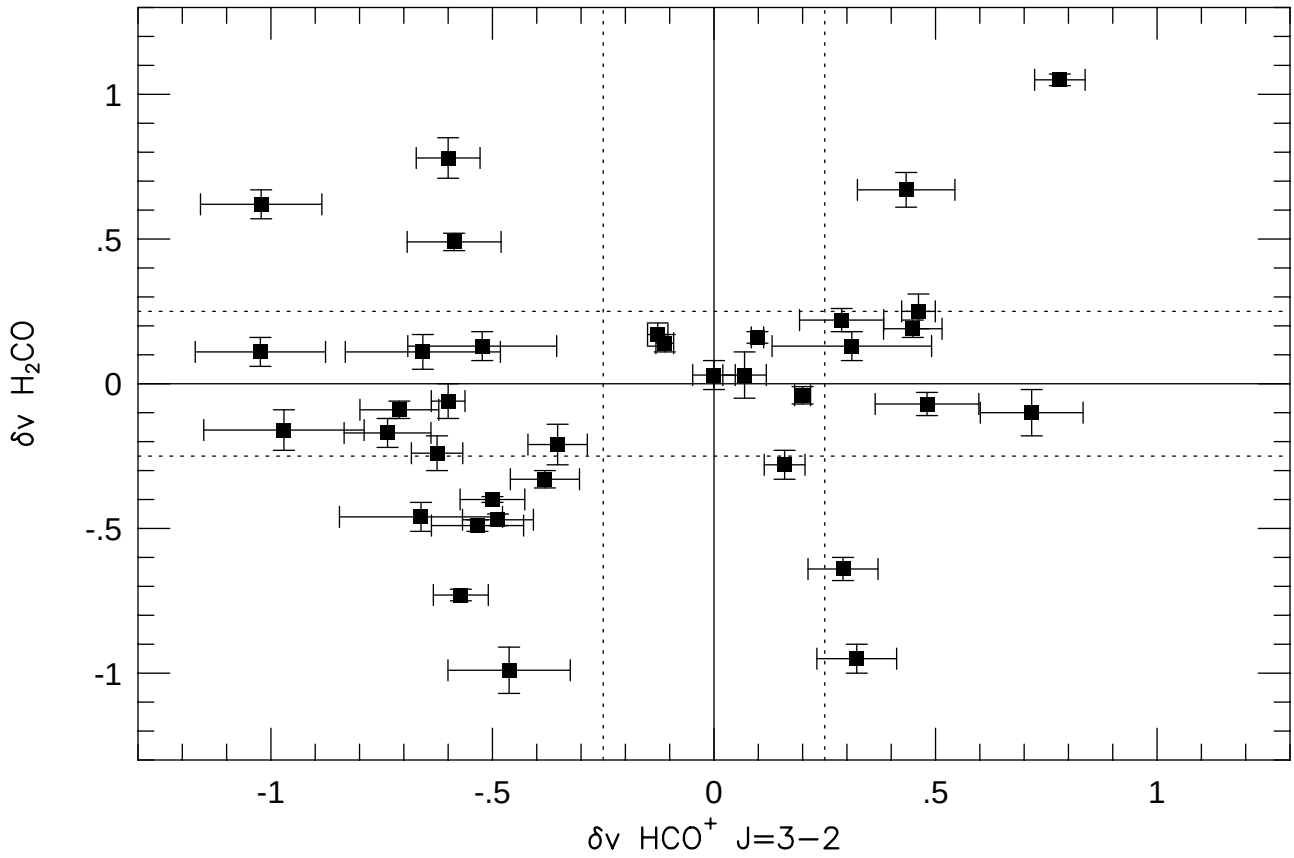
1
.5
0
-.5
-1
δv H2CO
-1
-.5
0
.5
1
δv HCO+ J=3−2

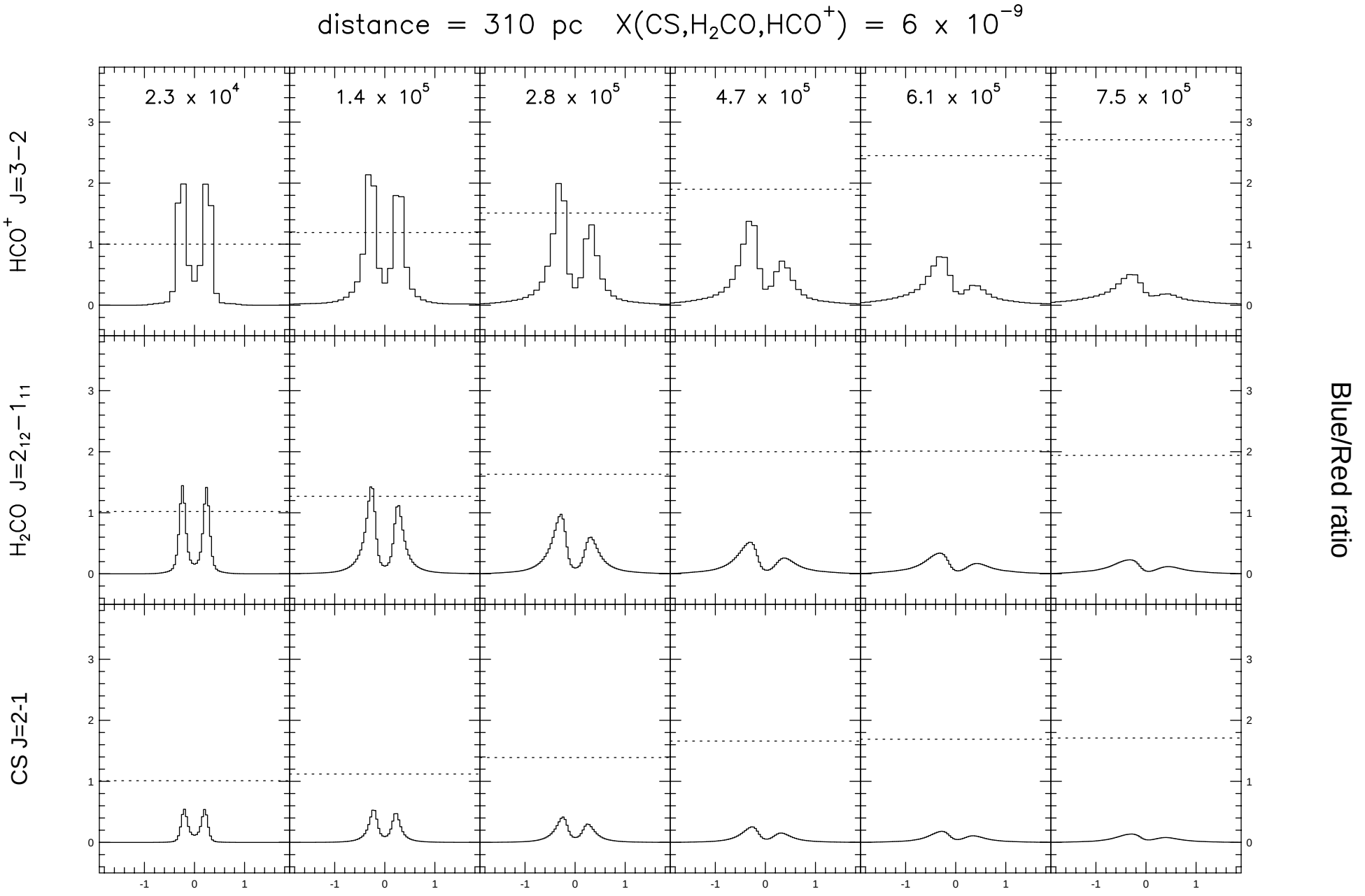
distance = 310 pc X(CS,H2CO,HCO+) = 6 x 10-9
2.3 x 10^4
1.4 x 10^5
2.8 x 10^5
4.7 x 10^5
6.1 x 10^5
7.5 x 10^5
HCO+ J=3−2
H2CO J=2_12−1_11
CS J=2-1
Blue/Red ratio